Quaternary Geochronology 84 (2024) 101613

Contents lists available at ScienceDirect

Quaternary Geochronology

journal homepage: www.elsevier.com/locate/quageo

Quartz luminescence sensitivity enhanced by residence time in the critical zone

Natalie M. Tanski [a,*], Tammy M. Rittenour [a], Francesco Pavano [b,c], Frank Pazzaglia [b], Jenna Mills [a], Lee B. Corbett [d], Paul Bierman [d]

[a] Department of Geosciences, Utah State University, Logan, UT 84322, USA
[b] Department of Earth and Environmental Sciences, Lehigh University, Bethlehem, PA 18015, USA
[c] Now at Department of Earth, Environment and Resources Sciences, University of Naples, Federico II, Napoli, 80126, Italy
[d] Rubenstein School of the Environment and Natural Resources, University of Vermont, Burlington, VT 05405, USA

ARTICLE INFO

Keywords:
Quartz luminescence sensitivity
Surface processes
Critical zone
Magnetic susceptibility
Chemical weathering indices
^{10}Be erosion rates

ABSTRACT

The emerging use of quartz luminescence properties to characterize Earth-surface processes shows promise, with optically stimulated luminescence (OSL) sensitivity proposed as a valuable tool for provenance or sediment history tracing. However, the geologic processes that lead to quartz sensitization remain unclear. Here we study the impact of source rock and surface processes on the luminescence properties of quartz sand from bedrock and modern and Late Pleistocene alluvium generated from a mountainous catchment in northern Utah, USA. Continuous wave and linear modulated OSL are used to characterize the luminescence sensitivity and intensity of the fast-decay component. We compare the OSL sensitivity with sand-grain provenance and with proxies for surface processes such as topographic metrics, cosmogenic ^{10}Be-derived erosion rates, chemical weathering indices, and magnetic susceptibility. Late Pleistocene sediment has low OSL sensitivity and a weak fast-decay component, similar to bedrock samples from the source area. In contrast, modern alluvium is dominated by the fast-decay component and has higher and more variable OSL sensitivity, with no clear relationship to upstream bedrock source. There is, however, an inverse relationship between OSL sensitivity and catchment-averaged erosion rates and a positive relationship with chemical weathering indices and magnetic susceptibility. These metrics suggest that the modern alluvium has experienced increased residence time in the shallow critical zone compared to the Late Pleistocene sediments. We suggest that changes in hillslope processes between the effectively wetter, cooler Pleistocene and the dryer, warmer conditions of the Holocene enhanced the luminescence properties. The results suggest that climatic controls on rates and processes of chemical and mechanical weathering and sediment transport and residence within the critical zone are encoded in the luminescence properties of quartz sand.

1. Introduction

Luminescence dating provides an age estimate of the time since quartz or feldspar grains were last exposed to light or heat (Huntley et al., 1985; Aitken, 1998). Quartz luminescence dating is a useful tool in Quaternary research because of its abundance across the Earth's surface. The luminescence phenomena within quartz are related to the trapped charge in defects within the crystalline structure. Electrons are stored until the mineral is exposed to sufficient energy (optical, thermal, or mechanical) to release the trapped electrons (e.g., Bailey, 2001; Preusser et al., 2009). Luminescence (photons) is emitted upon recombination at a lower energy state. The intensity of the natural luminescence signal of a sample is related to the absorbed ionizing dose of radiation accumulated during burial (as a function of dose rate and burial duration) and the sensitivity of the mineral to acquire a luminescence signal. Optically stimulated luminescence (OSL) sensitivity is defined as the photon counts produced per Gray of absorbed dose per sediment volume or mass (Wintle and Murray, 1999). Quartz with high OSL sensitivity dominated by the fast-decay component is required for luminescence dating (Moska and Murray, 2006; Murray et al., 2021). However, there remains much to learn about the geologic processes that lead to quartz sensitization of the fast-decay component (e.g., Moska and Murray, 2006; Sawakuchi

* Corresponding author.
E-mail address: natalie.tanski@usu.edu (N.M. Tanski).

https://doi.org/10.1016/j.quageo.2024.101613
Received 31 December 2023; Received in revised form 2 August 2024; Accepted 5 August 2024
Available online 8 August 2024

et al., 2011).

OSL sensitivity is thought to be inherited from source rock properties (Fitzsimmons, 2011; Sawakuchi et al., 2011) or acquired and modified by weathering, erosion (e.g., Sawakuchi et al., 2018; Dave et al., 2022), transport processes (e.g., Pietsch et al., 2008; Gliganic et al., 2017), or heating by wildfire (e.g., Phinney, 2022; Zhang et al., 2023b). The goal of this research is to test these competing ideas by investigating relationships between OSL sensitivity, upstream bedrock sources, and proxies of surface processes in a catchment. We measure catchment-averaged erosion rates via in-situ terrestrial cosmogenic nuclide ^{10}Be in quartz sand and proxies of weathering intensity using chemical alteration indices and magnetic susceptibility of the same alluvial samples. Contributing source-area provenance is determined based on geologic mapping and the percentage of upstream contributing bedrock types using a Geographical Information System (GIS) and sand petrography. We measure continuous wave OSL (CW-OSL) sensitivity and analyze the fast-decay component using linear modulated OSL (LM-OSL) on quartz grains sampled from Pleistocene and modern fluvial-deltaic deposits and bedrock quartzites exposed in the catchment.

If quartz OSL sensitivity is related to bedrock source, then luminescence properties should generally follow spatial changes in the rock types in the upstream contributing area. If OSL sensitivity is related to transport distance, then the furthest downstream sites should have higher OSL sensitivity. However, if OSL sensitivity is dependent on residence time within the critical zone, then luminescence properties should scale inversely with erosion rates and directly with indices sensitive to chemical leaching of the sediment during hillslope storage and exposure to critical zone processes. The critical zone is defined as the "near surface environment that involves interactions between rock, soil, water, air, and living organisms" (NRC, 2001). Finally, if climate-controlled surface processes dictate OSL sensitivity, then luminescence properties are expected to be different between glacial and interglacial mean climate states (Late Pleistocene versus Holocene).

2. Background

The innate properties of quartz minerals that affect OSL sensitivity can be linked to the type and density of defects within the crystal lattice, the opening of deep hard-to-bleach traps that have long retention lifetimes, and/or the increase of the luminescence centers available to receive electrons and generate luminescence (e.g., Bailey, 2001). Defects are thought to be related to the intrinsic geologic characteristics and history of quartz minerals, such as rock formation and deformation history (Bøtter-Jensen et al., 1995; Preusser et al., 2009). The pressure and temperature during quartz crystallization impacts the incorporation of trace elements, and substitution of Si^{4+} by other cations (e.g., Al^{3+} or Ti^{4+}) that can attract and retain trapped charge (electrons) (Larsen et al., 2004; Wark and Watson, 2006; Preusser et al., 2009). In converse, the incorporation of H_2O in the mineral structure during crystallization causes the elimination of luminesce centers (Hashimoto et al., 2003; Tajika and Hashimoto, 2006). Additional defects may be activated or produced by irradiation or heating and can function as electron traps that store trapped charge or luminescence centers that produce photons upon electron recombination at a lower energy state (such as an electron vacancy) (Aitken, 1998; Preusser et al., 2009). Thermal annealing experiments suggest that increased OSL sensitivity with heating is generated by emptying of deep, tightly bound, traps and the enhancement of luminescence centers (Bøtter-Jensen et al., 1995; Bailey, 2001; Galloway, 2002). Although mineral-lattice defects or chemical impurities are dependent upon conditions during mineral formation or diagenesis and alteration, subsequent exposure of quartz minerals to optical, thermal, or mechanical energy may free electrons in deep traps and provide new luminescence centers, thereby enhancing OSL sensitivity (e.g., Moska and Murray, 2006; Pietsch et al., 2008; Mineli et al., 2021).

Due to differences in quartz OSL sensitivity between source rocks it has been proposed as a sediment provenance tool (e.g. Gray et al., 2019; Nian et al., 2019; Lu et al., 2021; Alexanderson, 2022; Capaldi et al., 2022; Goswami et al., 2023; Souza et al., 2023; Zhang et al., 2023a). However, quartz derived directly from crystalline bedrock typically has lower OSL sensitivity than quartz from transported sediment or sedimentary bedrock (Chithambo et al., 2007; Sawakuchi et al., 2011; Jeong and Choi, 2012; Guralnik et al., 2015) suggesting that quartz sensitization is enhanced by the exposure to surface processes, increasing its original bedrock-derived signature. Sensitization has been proposed to be a function of repeated exposure to radiation during burial and sunlight during sediment transport in fluvial settings (Pietsch et al., 2008; Gliganic et al., 2017) and in laboratory experiments (Bøtter-Jensen et al., 1995; Moska and Murray, 2006; Pietsch et al., 2008; Tsukamoto et al., 2011). The history of irradiation-bleaching cycles may therefore give rise to differences in OSL sensitivity. For example, the transport history between fluvial, aeolian, lacustrine, colluvial, or glacial sediment can impart different OSL sensitivity (Li and Wintle, 1992; Fuchs and Owen, 2008; Fitzsimmons et al., 2010; Sawakuchi et al., 2011). Fluvial, aeolian, and coastal sediments are suspected to have greater OSL sensitivity than the other settings due to the repetition of irradiation-bleaching cycles during transport.

OSL sensitivity may scale with denudation rates and sediment storage or transport time (Sawakuchi et al., 2018). Quartz derived from young, high-relief mountain ranges typically is not dominated by the fast-decaying OSL component (e.g., Rhodes, 2000; Klasen et al., 2007; Palamakumbura et al., 2016). Under high uplift rates, erosion and transport of sediment is rapid enough that quartz grains may not be exposed to as many sediment transport cycles as sediment derived from low-uplift areas. Quartz sourced from stable landscapes with well-developed soils, like the Amazonian Shield or the Chinese Loess Plateau, have high sensitivity suggesting that quartz residence time in soils or exposure to weathering processes at the surface may also enhance quartz sensitization (e.g., Sawakuchi et al., 2018; Dave et al., 2022; Souza et al., 2023). Although, chemical weathering intensity alone does not seem to be correlated to OSL sensitivity within a soil profile (Cao et al., 2022) and *in-situ* sourced quartz from saprolites lack a fast-decay component compared to transported sediment (alluvium or colluvium) within the same soil profile (Nelson et al., 2022). These observations suggest that luminescence characteristics are encoded by the duration and types of weathering and transport processes that quartz grains have been exposed to at the Earth's surface.

3. Regional setting

3.1. High Creek catchment

Samples for OSL sensitivity were collected from High Creek in northern Utah, USA. The High Creek catchment is small (52 km^2), exposes quartzites, and contains Late Pleistocene and modern fluvial sediments, making it a suitable site to test for bedrock and geomorphic controls on OSL sensitivity. The catchment drains the Bear River Mountains into Cache Valley, part of the extensional Basin and Range Province (Fig. 1). The catchment has a maximum elevation of 3.5 km and 1.6 km of relief. High Creek drains towards the west, perpendicular to the normal fault-bounded range front and has two major tributaries, the North Fork, and the South Fork. The South Fork hosted a cirque glacier in the Pleistocene (DeGraff, 1976). The catchment is underlain by Proterozoic to Silurian sedimentary and meta-sedimentary units dominated by silty limestone and quartzite (Dover, 2007, Fig. 1). The slip rate on the northern end of the East Cache Fault is unsteady, however it is thought to be 100–500 m Myr^{-1} (Evans, 1991) and a fault scarp in Late Pleistocene alluvium suggest the most recent rupture event occurred after ~16 ka (McCalpin, 1994).

Pleistocene deposits sourced from the High Creek catchment are preserved as coarse-grained Gilbert-type deltas with prograding foresets

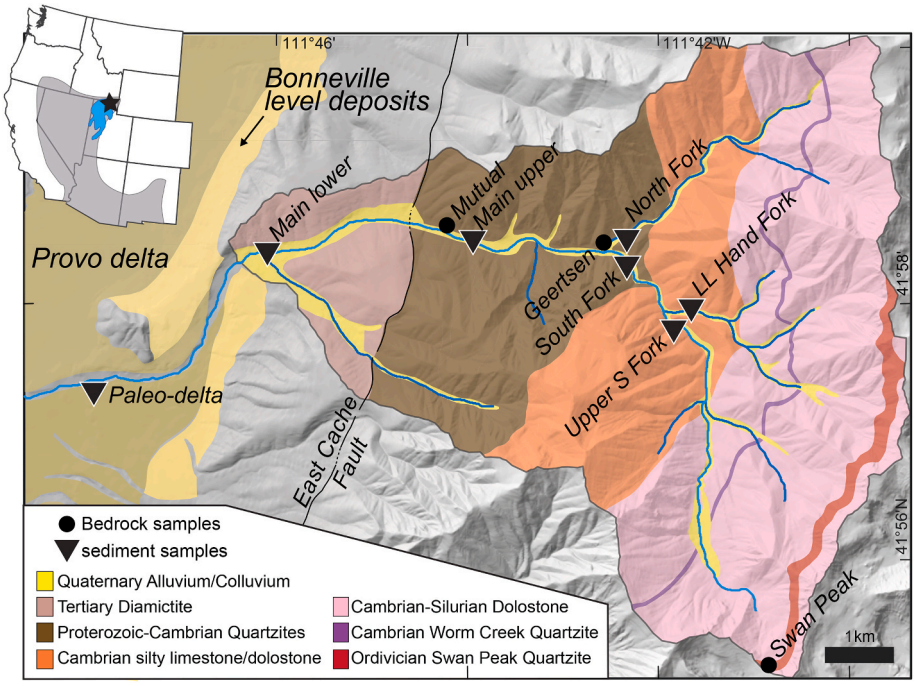

Fig. 1. Geologic map of High Creek and locations of samples and key features discussed in the text. Geologic information is modified from Dover (2007). Inset show's location of High Creek (black star) within Lake Bonneville (blue) in the Basin and Range Province (gray) of the western United States.

that formed in pluvial Lake Bonneville on the subsiding hanging wall of the East Cache Fault (Fig. 1). Well-preserved shorelines within the basin document two prominent lake levels, the Bonneville, and Provo levels (Gilbert, 1890). Transgression of Lake Bonneville began ~30 ka and the Bonneville highstand was short lived due to catastrophic outburst flooding at ~18 ka, when the water level within the closed basin reached a spillover divide (Gilbert, 1890; Oviatt et al., 1992; Godsey et al., 2005; Oviatt, 2015). The lake restabilized at the Provo level for approximately 3 kyr (18–15 ka) (Godsey et al., 2011; Oviatt, 2015; Miller et al., 2015). Lake levels dropped to near the modern Great Salt Lake level by the early Holocene due to climate-driven reduced effective moisture (Oviatt et al., 1992).

The lower reach of High Creek cuts through paleo-delta deposits constructed during both the Bonneville and the Provo stages. A quarry southwest of the mouth of the canyon exposes prograding foresets of the Provo-level delta, which downlap onto older, fine bottomset pro-delta beds of the Bonneville-stage delta (Fig. S1).

3.2. Late Pleistocene versus Holocene climate in the Basin and Range

Fluvial samples from two end-member climate states were sampled to test for the influence of climate-mediated controls on quartz sensitization; cold, dry Late Pleistocene with higher effective moisture and the warmer, drier Holocene (Thompson et al., 2016). The Basin and Range contained over one hundred Late Pleistocene pluvial lakes that formed under cooler conditions with less evaporation (Belanger et al., 2022), with Lake Bonneville being one of the largest pluvial lakes in the region. Pluvial lakes generally reached highstand position when local glaciers were at their maximum extent because of similar climatic influences on the glacial ice mass balance (García and Stokes, 2006; Matsubara and Howard, 2009; Lyle et al., 2012). Lake highstands broadly correspond to the Last Glacial Maximum (LGM) and cool sea-surface temperatures in the North Atlantic during Heinrich stadial 1 (Heinrich, 1988; Munroe and Laabs, 2013). Pluvial lake levels rapidly decreased due to decreased effective moisture in the Holocene, indicating climatically sensitive watersheds across the Basin and Range (Godsey et al., 2005). Aridification was driven by orbital changes in solar insolation and a northward shift of the jet stream during deglaciation (Benson and Thompson, 1987; García and Stokes, 2006).

Critical-zone processes in the High Creek catchment likewise differed between the Late Pleistocene and Holocene. Climate is considered a primary control on hillslope vegetation, rock weathering, erosion, and transport capacity within a watershed (Gilbert, 1877; Bull, 1991). The South Fork hosted a small cirque glacier and periglacial processes were likely active in High Creek during the last glacial period, which would have increased frost-driven sediment production leading to accumulation of colluvium on hillslopes (Whitney and Harrington, 1993; Marshall et al., 2015, 2021). Due to the enhanced physical weathering, there would have been more efficient sediment production and transport (Anderson et al., 2013; Marshall et al., 2017). In contrast, modern hillslopes have a thin soil cover and are likely more vegetated than in the Late Pleistocene (e.g., Louderback and Rhode, 2009; Louderback et al., 2015; Thompson et al., 2016).

4. Materials and methods

4.1. Research design

We leverage the spatial and temporal characteristics of the High Creek catchment to test for surface process and source-rock influence on OSL sensitivity. Our sampling strategy focused on three primary areas: the modern channel, the Late Pleistocene paleo-delta, and the surrounding bedrock. We sampled modern alluvium from sandy mid-channel bars and active riverbanks along the High Creek drainage to test if OSL sensitivity is related to transport distance of the grains and changes in upstream bedrock source. Four samples were collected from upstream of the confluences of the largest tributaries and two samples were collected downstream along the lower mainstem of High Creek (Fig. 1). The lower mainstem sample (Main lower) is the furthest downstream site and represents a similar sediment contribution from the catchment area that fed the paleo-delta (Fig. 1). In contrast, we collected samples from the Late Pleistocene paleo-delta to address if climate-modulated changes in Earth-surface processes are related to the luminescence properties. Four samples were collected from the Late

Pleistocene delta, three at ~25 m intervals within prograding foresets of the Provo lake stage, and one from stratigraphically older pro-delta fine sands (Fig. S1). Bedrock samples from within the High Creek catchment were collected to test for the influence of bedrock provenance on the downstream alluvial sediment. Source rock samples include quartzites of the Ordovician Swan Peak Formation, Neoproterozoic Upper Geertsen Canyon Formation, and the Cambrian Mutual Formation (Fig. 1). We compare quartz OSL sensitivity of alluvial samples to other metrics of surface processes including ^{10}Be-derived erosion rates, magnetic susceptibility, and chemical weathering indices.

4.2. Luminescence sample collection and processing

Bedrock samples were collected from outcrop exposures and crushed in a jaw crusher to disaggregate into sand-sized grains. Samples from the paleo-delta were collected in metal tubes so they could be used for both quartz OSL dating and sensitivity analyses. Alluvial samples from river channel bars were collected in clear bags. All samples were wet sieved to the 150–250 μm sand fraction to preferentially select fluvial-transported sediment and minimize potential confounding effects of distal-sourced and finer grained aeolian sediment. The quartz sand was isolated using treatment with 30% HCl and 3% H_2O_2 to remove carbonates and organic matter. Sodium polytungstate (2.7 g/cm^3) was used to separate quartz from heavy mineral grains. Grains were etched in 48% HF and 30% HCl to remove the alpha irradiated rim of the quartz grains, to remove feldspar grains, and to prevent fluorite precipitation.

4.3. Luminescence measurements

Late Pleistocene samples from the delta were dated following the single-aliquot regenerative dose (SAR) protocol (Murray and Wintle, 2000). Procedures regarding luminescence dating are included in the supplement. All luminescence measurements were performed at the Utah State University Luminescence Laboratory on a Risø OSL/TL DA-20 instrument with blue LEDs (470 ± 30 nm) and a detection through 7.5 nm UV filters (U-340) (Bøtter-Jensen et al., 2003). See Table S1 for the sequence protocol used for dating and Table S2 for the acceptance criteria used to filter aliquots for equivalent dose (D_e) determination. The D_e's are calculated using a weighted mean or the minimum age model (MAM) (Galbraith et al., 1999; Galbraith and Roberts, 2012) from at least 15–20 small aliquots (1–2 mm, ~20–80 grains). The equivalent doses are below the characteristic dose of saturation (Table S3 and Fig. S2) and a dose-recovery test illustrates that the artificial D_e's are recoverable within ~8% (Table S4). Radio-isotope concentrations of the sediment surrounding each sample were measured by ICP-MS/OES methods for calculation of dose rates using the DRAC online calculator (Durcan et al., 2015). Dose-rate information is included in the supplement (Table S5). A moisture content of 5 ± 2 % was considered to be representative of the burial history.

Aliquots of 2 mm in diameter (~80 grains with perfect packing) were mounted on stainless steel discs. The natural signal was first optically bleached and then each aliquot was given ~20 Gy of dose using a ^{90}Sr/^{90}Y beta source with a dose rate of 0.09–0.1 Gy s^{-1} (see Table 1 for details). A preheat test determined that OSL sensitivity is independent of preheat temperature over the range of 200–275 °C (see Fig. S3), therefore a preheat temperature of 240 °C was chosen to remove signals from thermally unstable shallow traps (i.e. the 110 °C trap). All aliquots were checked for quartz purity using infrared (IR) stimulation to test for feldspar contamination for both OSL dating and sensitivity analyses. We rejected aliquots with an IR response signal (first 0.6s) that was three times the background signal (mean of the last 5s). This is our only rejection criteria for the aliquots measuring OSL sensitivity. OSL sensitivity analyses incorporated data from 15 accepted aliquots per sample. All OSL sensitivity values were measured on the same instrument using the same grain size (150–250 μm), aliquot volume (2 mm, ~80 grains), and applied dose (~20 Gy) for each sample. Preheat treatments at 240 °C for 10 s were applied before all OSL measurements (Table 1).

Table 1
Optically Stimulated Luminescence Sensitivity sequence procedure.

Step	Treatment	Purpose
1	Illumination with blue-green LED (470 nm @ 56 mW cm^{-2}) at room temperature (0 °C) for 100s	Bleach natural signal
2	Beta irradiate 200s	~20 Gy lab dose
3	Preheat at 240 °C for 10 s	Eliminate unstable signals
4	Infrared LED (875 nm) stimulation at ~20 °C for 40s	Test for feldspar contamination
5	Blue-green LED (470 nm @ 56 mW cm^{-2}) stimulation at 125 °C for 40s	CW-OSL sensitivity[a] and calculation of the fast-ratio
6	Repeat 2-4	
7	Blue-green LED (0–80 mW cm^{-2}) stimulation at 125 °C for 1000s	LM-OSL sensitivity[b]

[a] The CW-OSL sensitivity is the first 0.6 s of light stimulation minus the average background over the last 3 s of signal decay.
[b] The LM-OSL fast-decay sensitivity was measured as the integrated signal over 16–32 s of stimulation with a background subtraction collected from blank discs.

The quartz OSL sensitivity was calculated using continuous wave OSL (CW-OSL) and Linear-Modulated OSL (LM-OSL) measurements. The CW-OSL sensitivity was calculated as the signal from the first 0.6 s of light stimulation minus the average background signal over the last 3 s of signal decay, per the applied radiation dose per aliquot volume. The fast-ratio, a metric that compares the intensity of the fast and medium-decay components, was used as another measure of the strength of the fast component in the CW-OSL curve (Durcan and Duller, 2011). See Table S6 for values used in this calculation. Durcan and Duller (2011) suggest that samples with a fast-ratio >20 are dominated by the fast-decay component.

The LM-OSL signal was acquired to determine the relative contribution of the fast component to the total quartz OSL signal (Bulur et al., 2000). LM-OSL was measured over 1000s and 250 data channels from 0 to 100% LED power (max 80 mW cm^{-2}) following a ~20 Gy dose after the CW-OSL (Table 1). LM-OSL curves from 15 aliquots were averaged for each alluvial sample for single component analysis. The LM-OSL curves were separated into first order components using function fit_LMCurve in R "luminescence" package (Kreutzer et al., 2023). The curve deconvolution gives values for peak intensity and position for each component following Kitis and Pagonis (2008). The R determined fast-decay peak position was between 24 and 27 s for most alluvial samples (Figs. S4d–f). We define the fast decay signal from the LM-OSL curve as the integrated signal over 16–32 s (1–3 mW cm^{-2}) of stimulation with a background subtraction collected from blank discs normalized by applied dose and aliquot volume.

4.4. Geologic source and quartz petrography

The relative proportions of geologic units grouped by lithology within the contributing areas of each sample were calculated using GIS. Contributing areas for each sample were delineated using a 10 m digital elevation model and lithologic units were masked using the 1:100,000 scale digital Geologic Map of the Logan 30 x 60 quadrangle (Dover, 2007). Quaternary-surficial map units were ignored for bedrock source area calculations because they are assumed to have been sourced from the same bedrock as the modern river sands. Geologic units within the catchment were simplified to isolate quartzites and combine the limestones and dolostones that contribute little or no quartz. Representative grain mounts of untreated but sieved (150–250 μm) samples were assessed petrographically to reveal any differences in the characteristics of the quartz grains between samples.

4.5. Catchment metrics

Terrain metrics for the contributing areas of samples along High Creek were calculated using the TAK and TopoToolbox 2 MATLAB packages (Schwanghart and Scherler, 2014; Forte and Whipple, 2019). Metrics include contributing drainage area, fluvial transport distance, and the mean relief and slope of contributing areas.

4.6. In-situ ^{10}Be derived erosion rates

Catchment-wide denudation rates are determined by measuring the concentration of the *in-situ* produced cosmogenic nuclide ^{10}Be in quartz within alluvial sediment (Brown et al., 1995; Bierman and Steig, 1996; Granger et al., 1996). Some consider such erosion rates are integrated over the time it takes for upper 0.6 m (one e-folding depth) of bedrock (density of 2.7 g cm^{-3}) to be removed upstream of the alluvial sample collection point (von Blanckenburg, 2005); however, the penetration depth of less attenuated muons and some neutrons means that samples are influenced by erosion rates farther back in time. The 250–850 μm fraction of each luminescence sample was processed for measurement of ^{10}Be concentration. However, only samples from the delta, upper High Creek, North Fork and upper South Fork yielded enough quartz for Be extraction and accelerator mass spectrometry analyses.

We isolated Be from quartz at the National Science Foundation/University of Vermont Community Cosmogenic Facility using the methods described in Corbett et al. (2016). We added ~250 μg of ^{9}Be to each sample (using a carrier with a Be concentration of 304 μg g^{-1}), digested the quartz in hydrofluoric acid, and performed anion and cation column chromatography to isolate and purify Be. Samples were measured by accelerator mass spectrometry at the Purdue Rare Isotope Measurement Laboratory and were normalized to primary standard 07KNSTD3110 (Nishiizumi et al., 2007). Samples were corrected for backgrounds using process blanks and we calculated erosion rates using an online exposure age calculator (Balco et al., 2008). Erosion rates were calculated assuming the central basin latitude and longitude and mean elevation, while also accounting for isotope decay within the paleo-delta, and no correction for topographic shielding (e.g., Granger et al., 1996). Calculations showed that production after deposition and at depth in the delta were low, on the order of at most a few thousand atoms per gram. Additional details about isolating the quartz fraction, purifying Be, isotope measurements, and calculations of the erosion rate are included in the supplemental materials.

4.7. Magnetic susceptibility

Magnetic susceptibility (m^3 kg^{-1}) is a measure of the magnetic strength of all the ferromagnetic and paramagnetic minerals in sediment. Magnetic mineralogy has been widely used as a rock-magnetic proxy of long-term and/or orbitally-driven climatic changes in catchment siliciclastic output (e.g., An et al., 1991; Clift, 2006; Gunderson et al., 2012). Extensive high-resolution sampling of the Chinese Loess Plateau has shown that magnetic susceptibility increases during episodes of soil development, likely driven by dust flux and the pedogenic production of ferromagnetic minerals and is therefore used as an index for assessing the degree of pedogenesis (e.g., An et al., 1991; Lü et al., 2014). Magnetic susceptibility is used here as a proxy for the relative recruitment of magnetically-rich hillslope sediment with respect to magnetically-poor, non-weathered bedrock. A uniform volume of mass-normalized sand fraction of samples (62.5–2000 μm) was used to measure magnetic susceptibility. The average magnetic susceptibility of each sample was calculated from three replicate measurements using a Kappabridge or a KT-10 handheld susceptibility meter and converted to SI (m^3 kg^{-1}) units.

4.8. Proxies of chemical weathering

Chemical weathering intensity of a region can be estimated through elemental indices of soils and fluvial sediments (e.g., Nesbitt et al., 1980; Nesbitt and Young, 1982; Heimsath and Burke, 2013; Garzanti et al., 2014; Dinis et al., 2017). Geological provenance, weathering of source rocks, as well as geochemical and physical alteration of sediment during hillslope storage or transport all affect the proportion of labile and stable elements within sediment. Here chemical weathering indices are used as a proxy for residence time within the critical zone under processes of soil formation and chemical leaching.

We report the modified version of the Chemical Index of Alteration (CIA) and the Chemical Proxy of Alteration (CPA). The CIA calculates proportions of mobile (K, Na, Ca) to immobile Al, thus reflecting the weathering of feldspars (Nesbitt and Young, 1982). Since there are carbonates exposed within the catchment of High Creek, we modify the CIA to the CIX, which skips Ca, as in Garzanti et al. (2014). The CPA index reflects silicate weathering as a molar ratio between Al and Na, avoiding uncertainty in Ca sources and the K losses linked to illite formation from the weathering of smectite (Buggle et al., 2011). Other common raw elemental ratios used as chemical weathering proxies of mobile to less mobile elements include K/Al, K/Ti, Rb/Sr, Mg/Al (Nesbitt et al., 1980; Buggle et al., 2011; Hu et al., 2013). For evaluating the relative chemical weathering between samples, unprocessed subsets of all samples in the sand fraction (<2000 μm) were analyzed for elemental concentrations using standard ICP-MS methods.

5. Results

5.1. Luminescence geochronology

Luminescence age constraints on the paleo-delta range from 20.8 ka to 16.8 ka (Table 2). These ages are stratigraphically consistent with the sample placement in the delta sequence and align with published age models for the lake phases (Oviatt, 2015). The fine-grained pro-delta bottomset sands have a gaussian equivalent dose distribution (Fig. S2) and the weighted mean age is 20.8 ± 2.0 ka, consistent with the transgression of Lake Bonneville (Oviatt, 2015). Equivalent dose distributions from samples collected in prograding foresets are positively skewed (Fig. S2), which may be due to incomplete solar resetting of the natural

Table 2
Luminescence age information.

Sample	USU num.	Num. of aliquots[b]	Dose rate (Gy/kyr)[c]	De ± 2σ (Gy)	Age ± 1σ (ka)
Provo 48 m[a]	USU-3667	23 (47)	1.31 ± 0.05	21.98 ± 3.02	16.80 ± 2.19[d]
Provo 25 m[a]	USU-3665	23 (45)	1.18 ± 0.05	20.07 ± 3.16	17.03 ± 1.89[d]
Provo 0 m[a]	USU-3664	23 (50)	1.24 ± 0.05	21.49 ± 2.51	17.35 ± 1.82[d]
Bonneville	USU-3666	16 (33)	1.22 ± 0.05	24.70 ± 2.30	20.79 ± 1.95[e]

[a] Length refers to distance of progradation in the Provo foresets.
[b] Number of aliquots used in age calculation and number of aliquots analyzed in parentheses.
[c] Data used for calculating the dose rate is included in Table S5 in the supplement.
[d] Equivalent dose (D_e) calculated using the minimum age model (MAM) of Galbraith et al. (1999).
[e] Equivalent dose (D_e) calculated using a weighted mean.

OSL signal (partial bleaching) prior to deposition in the source-proximal delta. We preferentially use the minimum age model (MAM) for calculation of the equivalent dose for the foreset samples due to the skew in equivalent dose values and because MAM ages are more consistent with the geomorphic position of the paleo-delta at the Provo lake stage. The MAM-OSL ages from the foreset beds are 17.3 ka to 16.8 ka and are consistent with expected ages of stability during the Provo level, 18-15 ka (Oviatt, 2015). The OSL age model from the delta foreset beds indicates a linear progradation rate of ~87 m kyr^{-1}. Additional details on the luminescence dating are included in the supplement.

5.2. Luminescence properties

We report quartz OSL sensitivity for the Pleistocene and Holocene alluvium and bedrock samples (Table 3 and Fig. 2). Mean values of sediment samples range from 61 ± 3 counts Gy^{-1} mm^{-3} (Provo 25 m, Pleistocene paleo-delta) to 484 ± 96 counts Gy^{-1} mm^{-3} (North Fork, modern alluvium), while mean values of bedrock samples range from 31 ± 2 counts Gy^{-1} mm^{-3} (Geertsen) to 121 ± 10 counts Gy^{-1} mm^{-3} (Swan Peak). Kernel density estimate (KDE) plots of the OSL sensitivity of all aliquots per sample show low values with a unimodal distribution with a slight positive skew for both bedrock and Pleistocene sediments, while modern alluvial samples show a broader spread and higher OSL sensitivity values (Fig. 2). Bedrock samples have similar low OSL sensitivity values and distribution as the Late Pleistocene sediment samples. Modern alluvial samples typically have a few aliquots that plot near the low sensitivity values seen in the Pleistocene and bedrock KDEs. T-test analyses indicate that the quartz OSL sensitivity of Late Pleistocene samples are significantly different ($p < 0.05$) than modern alluvial samples, while some Late Pleistocene samples are statistically similar to bedrock samples (Table S7). Moreover, there is a positive relationship between the fast-ratio and the CW-OSL sensitivity (Fig. 3A). This relationship is expected since the CW-OSL sensitivity is based on the initial signal comprising the fast-decay component minus the background signal. The fast-ratio analysis demonstrated that 9% of bedrock aliquots, 33% of Pleistocene aliquots, and 85% of modern alluvial aliquots were dominated by the fast component as indicated by a fast-ratio >20.

LM-OSL curves representing the average of 15 aliquots per samples are shown in Fig. S4. The first peak in all LM-OSL curves represents a single component, which we interpret as the fast-decay component. The intensity of the fast component in the modern alluvial samples is up to an order of magnitude greater than the intensity of the Pleistocene samples (Fig. S4; Table 3). The fast-peak intensity from the LM-OSL curves show a power-law relationship with the CW-OSL sensitivity (Fig. 3B), confirming that both methods are a measure of the fast-decay component. The variance between peak intensity in the Pleistocene samples is less than those seen in the modern samples. Geertsen and Mutual Formations bedrock samples show no detectable signal in the fast-component, however the fast-component of the Swan Peak formation is similar to the Pleistocene samples.

5.3. Geologic source and quartz petrography

Modern samples have varying proportions of bedrock units in their contributing areas; however, the farthest downstream alluvial sample has the same upstream catchment as the Pleistocene delta samples (Fig. 2). Due to the prevalence of carbonate units within the High Creek catchment, quartz sand could only be derived from the thick Proterozoic-Cambrian quartzites that outcrop along the central part of the catchment area and the Swan Peak and Worm Creek quartzites that outcrop near the headwaters (Fig. 1). The upper S. Fork and LL Hand Fork only tap the thinner, headwater quartzites, while all other samples have additional contributions from the Proterozoic-Cambrian quartzites. The North Fork does not sample the Swan Peak quartzite.

Although samples vary in quartz provenance, petrography of the Pleistocene delta and modern stream sands reveals they share similar quartz-grain characteristics. All samples contain monocrystalline quartz with undulatory extinction, signifying ductile deformation (Fig. S5). Inclusions are common within quartz grains and present in all samples. Quartz grains commonly have secondary calcite precipitation on the rim of the grain. Grain shapes are generally sub-rounded to subangular and have mid-sphericity. Surface texture of grains commonly display conchoidal fractures.

5.4. Catchment metrics

The largest contributing drainage area is 50 km^2 for the delta and lower main-stem alluvial samples. The smallest contributing drainage area is the LL Hand Fork sample at 7.7 km^2. Transport distance varies from 3 km for the LL Hand Fork to up to 12 km for the lower Main sample. Counter to some assumptions of the processes that encode OSL sensitivity, the CW-OSL and LM-OSL sensitivity of the alluvium in High Creek decreases with transport distance downstream (Fig. 4). In addition, the mean OSL sensitivity decreases with increasing mean relief and shows no relationship to mean slope (Fig. S6).

5.5. In-situ ^{10}Be derived erosion rates

Denudation rates of upstream contributing areas derived from *in-situ* ^{10}Be concentrations range from 37 to 61 m Myr^{-1} (Table 4; Fig. 5A).

Table 3
Sample information and OSL sensitivity (n = 15 aliquots per sample).

Sample	Latitude, Longitude		Elevation (m)	CW-OSL sensitivity ± 1σ (counts Gy^{-1} mm^{-3})	Fast Ratio ± 1σ	LM-OSL fast-decay sensitivity± 1σ (counts Gy^{-1} mm^{-3})
Bedrock quartzites						
Geertsen	41.9747,	−111.7088	1835	39 ± 3	19 ± 7	97 ± 2
Mutual	41.9766,	−111.7334	1695	31 ± 2	7 ± 4	86 ± 2
Swan Peak	41.9187,	−111.6801	2798	121 ± 10	12 ± 1	147 ± 7
Late Pleistocene alluvium						
Provo 48 m	41.9559,	−111.7962	1451	72 ± 10	13 ± 2	135 ± 5.6
Provo 25 m	41.9560,	−111.7956	1443	61 ± 3	10 ± 1	132 ± 5.3
Provo 0 m	41.9560,	−111.7946	1457	119 ± 24	13 ± 2	173 ± 16.2
Bonneville	41.9558,	−111.7966	1434	107 ± 27	25 ± 4	158 ± 17.5
Modern alluvium						
Main lower	41.9764,	−111.7565	1585	375 ± 76 (1062 ± 374)[a]	142 ± 31 (244 ± 65) [a]	271 ± 43 (656 ± 209) [a]
Main upper	41.9759,	−111.7343	1715	335 ± 81	64 ± 36	235 ± 43
North Fork	41.9750,	−111.7084	1845	484 ± 96	28 ± 3	260 ± 59
South Fork	41.9744,	−111.7081	1845	368 ± 98	29 ± 4	251 ± 59
LL Hand Fork	41.9666,	−111.6978	1930	535 ± 101	116 ± 21	392 ± 76
Upper S. Fork	41.9658,	−111.6978	1930	454 ± 89	125 ± 36	355 ± 64

[a] Values only include aliquots within 2 standard deviations of the mean (n = 12). Values in parentheses include all aliquots (n = 15).

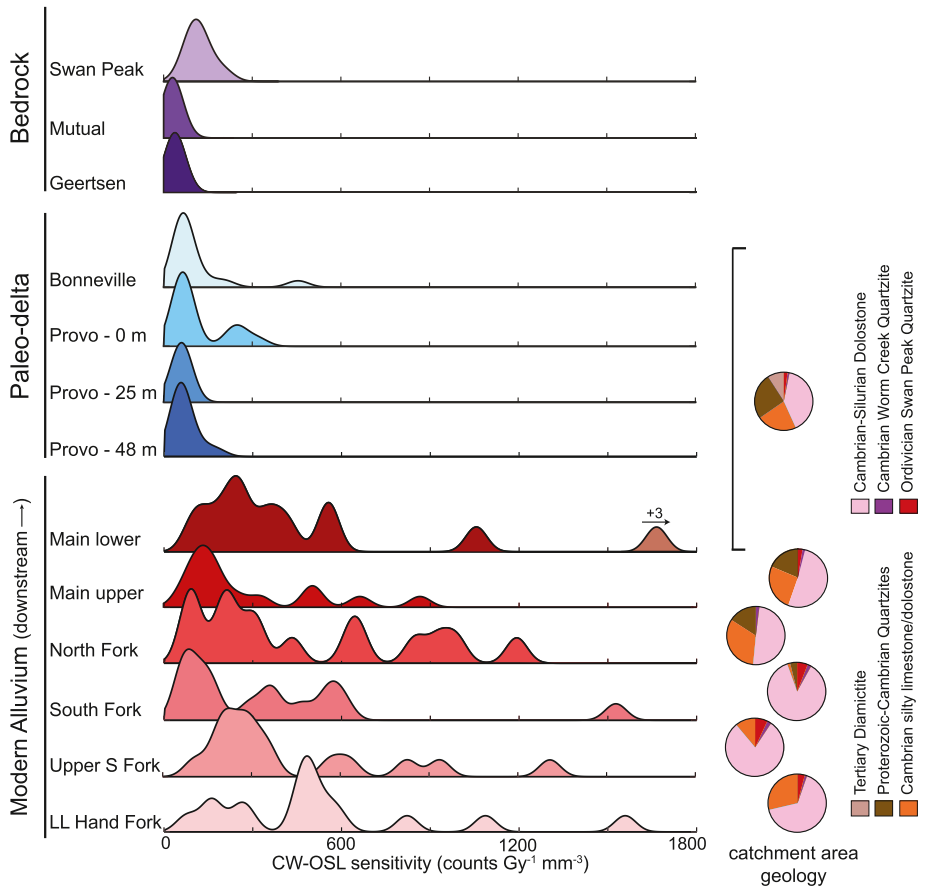

Fig. 2. Comparison diagram of quartz OSL sensitivity and catchment area geology for High Creek. Continuous-wave OSL (CW-OSL) sensitivity results plotted as kernel density estimates with a bandwidth of 36 counts Gy^{-1} mm^{-3}. The main lower sample includes three aliquots with OSL sensitivity values beyond the limit of the x-axis. Pie charts display the relative percentages of contributing bedrock for each sample. Colors match geologic units from Fig. 1.

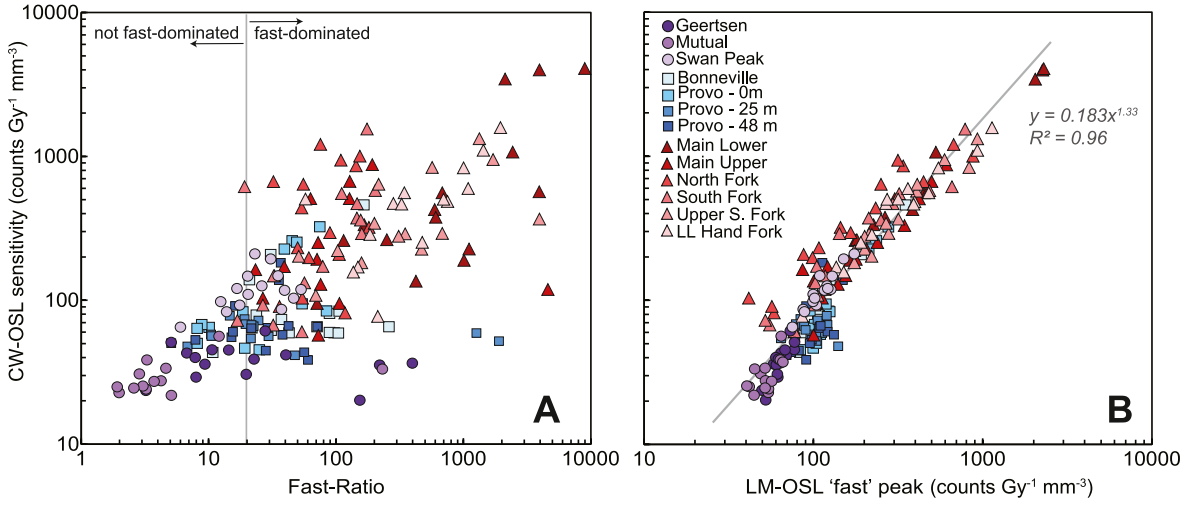

Fig. 3. (A) Plot of CW-OSL sensitivity versus the fast ratio for all aliquots. The vertical gray bar represents a fast-ratio value of 20, where samples that plot beyond this value are dominated by the fast-decay component. (B) Plot of CW-OSL sensitivity versus the fast-decay component measured from the LM-OSL curve. The positive relationship between the CW-OSL and LM-OSL supports the assumption that both are measuring the same fast-decay component.

Erosion rates from within the delta range from 52 to 61 m Myr^{-1} and are within uncertainties of each other. Samples from the Main Upper and North Fork have erosion rates of 46 ± 4 m Myr^{-1} and 37 ± 3 m Myr^{-1}, respectively. The upper South Fork has the highest measured erosion rate of 61 ± 6 m Myr^{-1}. The measured erosion rates are lower than fault displacement rates along the East Cache Valley fault, 100–500 m Myr^{-1} (Evans, 1991; McCalpin, 1994) and lower than erosion rates of 70–170 m Myr^{-1} recorded along the adjacent Wasatch Mountains (Stock et al., 2009).

5.6. *Magnetic susceptibility results*

Magnetic susceptibility values from all alluvial samples range from 2.5× 10^{-8} m^3 kg^{-1} to 11.5 × 10^{-8} m^3 kg^{-1} (Fig. 5B and Table 5).

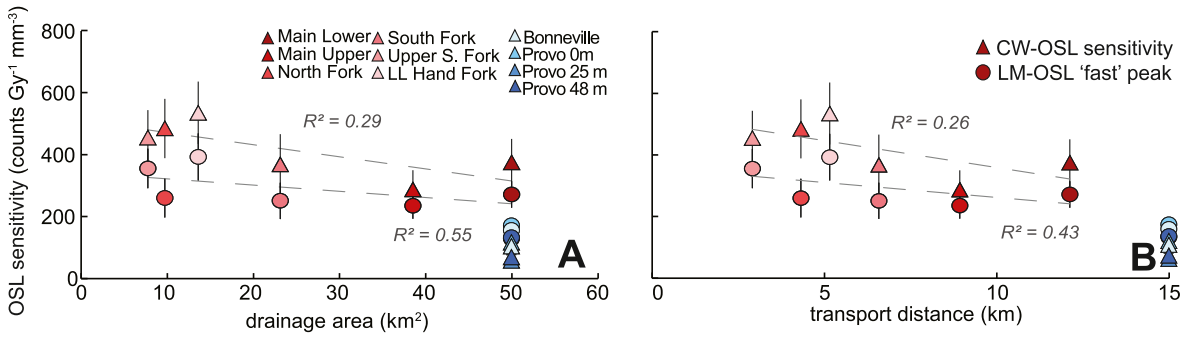

Fig. 4. CW-OSL ± 1σ sensitivity (circles) and fast-decay LM-OSL ± 1σ sensitivity (triangles) of the modern and Late Pleistocene alluvium versus upstream drainage area (A) and transport distance (B). The OSL sensitivity of modern alluvium decreases with upstream catchment area and transport distance. Colors correspond to sample location. Main Lower does not include the three high OSL sensitivity outlier aliquots.

Table 4
^{10}Be derived erosion rates.

Sample	[^{10}Be] (atoms g^{-1}) x 10^5	Erosion Rate[a] (m Myr^{-1})	Integration time[b] (kyr)
North Fork	4.15 ± 0.08	36.9 ± 3.1	16.4 ± 1.4
Upper S. Fork	2.64 ± 0.08	61.1 ± 5.6	9.9 ± 0.9
Main Upper	3.34 ± 0.08	45.6 ± 3.9	13.3 ± 1.1
Provo 0 m	3.89 ± 0.08	51.7 ± 4.4	11.5 ± 1.0
Provo 25 m	3.45 ± 0.07	57.1 ± 4.9	10.4 ± 0.9
Provo 48 m	3.24 ± 0.07	60.8 ± 5.2	9.8 ± 0.8
Bonneville	3.36 ± 0.09	58.4 ± 5.1	10.1 ± 0.9

[a] The CRONUS (version 3) on-line cosmogenic erosion rate calculator (Balco et al., 2008) was used to determine erosion rates. See Table S9 for more details on the parameters used to calculate erosion rates.
[b] The minimum interval of time over which the catchment-averaged erosion rates is measured (von Blanckenburg, 2005).

Pleistocene samples indicate that magnetic susceptibility increases up-section in the prograding foresets over an ~550 yr time span. The magnetic susceptibility of the Bonneville pro-delta sediments is within the range of magnetic susceptibility in the prograding foreset facies. The modern alluvium has uniformly stronger magnetic susceptibility than the Pleistocene delta sediment and shows little variance, consistent with a well-mixed hillslope soil source.

5.7. Proxies of chemical weathering

Pleistocene samples have low and similar CIX values of 66.5–67.4 while modern samples consistently have higher values of 70.7–72.8 (Fig. 5C and Table 5). There is a similar pattern between samples with CPA values (Fig. 5D and Table 5). Pleistocene samples are low, 86.8–89.2, while modern samples have greater values of 89.6–91.5. The one outlier in this dataset comes from the LL Hand Fork, which has lower CPA and CIX values than any alluvial sample. We suggest this might be due to a lack of silicates within the catchment. High CIX and CPA values indicate greater leaching of soluble or mobile cations and therefore suggest that the modern alluvium has experienced a longer weathering residence time in hillslope soils than Pleistocene sediment. Other ratios of mobile to resistant elements also indicate greater leaching in the modern sediment (K/Al, Mg/Al, Rb/Sr; Fig. S7). Elemental concentrations used are included in Table S10 in the supplemental material.

6. Discussion

Results from the High Creek catchment in northern Utah indicate that the OSL sensitivity of modern alluvial quartz is enhanced up to an order of magnitude compared to the Late Pleistocene delta sediment and bedrock samples. This pattern is seen in both the CW-OSL and LM-OSL sensitivity measurements for all samples. We infer what causes the observed patterns in quartz OSL sensitivity by examining the contributing bedrock source, the climatic conditions, and ties to critical zone processes.

A key observation from our research is that there are no clear links between bedrock source and OSL sensitivity (Fig. 2). The Main lower sample, which has a similar bedrock contribution as the samples collected from the Pleistocene delta, has significantly greater OSL sensitivity values than all four paleo-delta samples based on t-tests (see Table S7). In addition, there are no obvious petrographic distinctions among the quartz derived from the modern alluvium and the paleo-delta (Fig. S6), suggesting that the intrinsic geologic properties of the quartz grains are not a significant factor in the sensitization of the modern samples. Importantly, the luminescence properties of the Pleistocene samples are similar to the quartzite bedrock samples, in which both have weak OSL sensitivity and are not dominated by the fast-decay component (Figs. 2 and 3). Pleistocene deltaic samples are sourced from these quartzites up to 15 km upstream, indicating that transport in the Pleistocene did not significantly increase the sensitivity of quartz.

The results of this study demonstrate that the luminescence properties of modern sediments are enhanced compared to the Pleistocene sediment with no correlation to bedrock source requiring that the history of exposure to surface processes within the critical zone between the two time periods altered the luminescence properties. The ensuing discussion explores the influence of surface processes including sediment transport, chemical weathering, and physical erosion on luminescence properties.

6.1. Sediment transport

If OSL sensitivity is a function of transport distance, as suggested from other observational data (e.g., Pietsch et al., 2008; Gliganic et al., 2017), then the furthest downstream sample site would have the greatest OSL sensitivity due to exposure to more irradiation-bleaching cycles and the downstream increase in mechanical abrasion and sediment comminution. Considering just the modern alluvial sediments, the fast-component of the LM-OSL and the CW-OSL sensitivity show a weak negative relationship with increasing drainage area or distance from the headwaters (Fig. 4). Therefore, in the modern system, fluvial transport

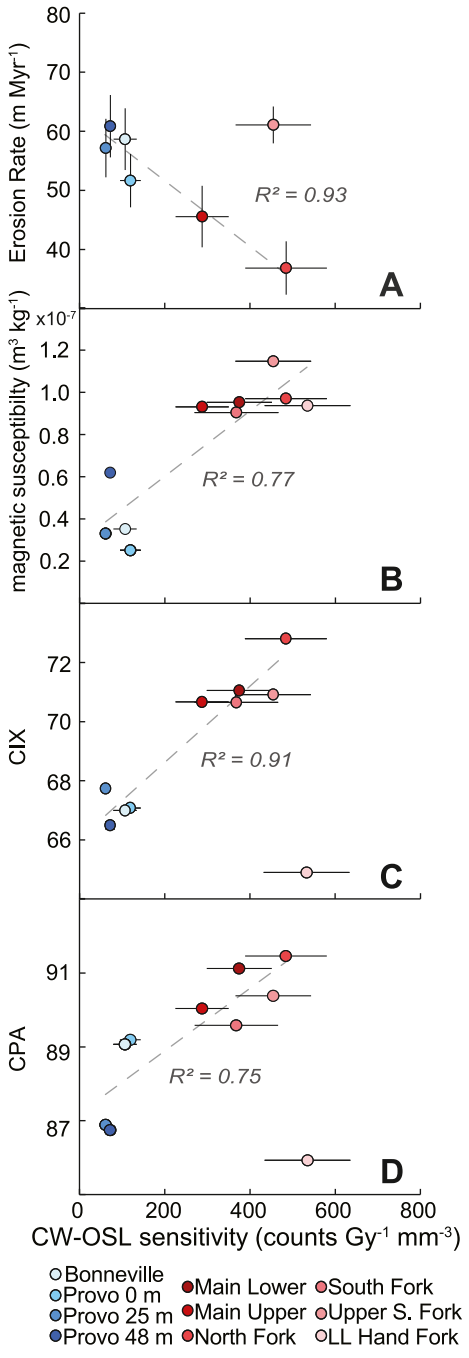

Fig. 5. CW-OSL ± 1σ sensitivity of modern and Pleistocene samples versus ^{10}Be catchment averaged erosion rate (A), magnetic susceptibility (B), the chemical index of alteration (C), and the chemical proxy of alteration (D). Colors correspond to sample location. Regression in (A) does not include the Upper S. Fork and regressions in (C) and (D) do not include the LL Hand fork. The Main Lower does not include the three high OSL sensitivity outlier aliquots.

time or distance is not a primary control on the enhancement of the fast-decay component of the quartz OSL signal. We hypothesize that the downstream decrease in OSL sensitivity observed in the modern sediments may result from the increased influx of quartz from outcrops near the lower drainage, quartz which may not share the same surface-process history as quartz derived from the headwaters. In addition, the Pleistocene delta samples are the furthest downstream sites; yet, they have the lowest OSL sensitivity of all alluvial samples. This suggests that transport distance is not a main contributor to the OSL sensitivity differences between the Pleistocene and modern sediments.

Table 5
Chemical weathering indices and magnetic susceptibility.

Sample	CIX	CPA	Magnetic susceptibility[a] (m^3 kg^{-1})
Provo 48 m	66.49	86.75	6.22 ± 0.04
Provo 25 m	67.74	86.89	3.31 ± 0.01
Provo 0 m	67.08	89.19	2.51 ± 0.02
Bonneville	67.00	89.07	3.57 ± 0.01
Main Lower	71.06	91.12	9.53 ± 0.37
Main Upper	70.67	90.04	9.31 ± 0.03
North Fork	72.81	91.46	9.70 ± 0.56
South Fork	70.65	89.58	9.05 ± 0.99
LL Hand Fork	64.90	85.93	9.37 ± 0.31
Upper S. Fork	70.92	90.38	11.5 ± 1.10

[a] The delta sediments were measured using a Kappabridge susceptibility meter whereas the stream alluvium was measured using a KT-10 handheld susceptibility meter; results are reproducible between instruments.

6.2. Physical and chemical weathering in the critical zone

The CW-OSL sensitivity has an inverse relationship with catchment-averaged erosion rates (Fig. 5A). Specifically, quartz from samples with greater OSL sensitivity also record greater *in-situ* ^{10}Be concentrations linked to slower erosion rates. The Upper South Fork does not fit this relationship and has the highest reported erosion rate. This sample was from the only sub-basin that was previously glaciated, suggesting that its increased erosion rate may relate to lingering effects of Late Pleistocene glacial erosion. Basin-scale erosion rates reflect the accumulation of ^{10}Be in quartz during shallow exposure within bedrock and its weathering products and during the production, storage, and transport of sediment in hillslope and fluvial systems (Granger et al., 1996). Therefore, the longer it takes for bedrock to be converted to sediment, traverse through the weathering zone as regolith, and undergo storage and transport before entering and being transported in the fluvial system, the more ^{10}Be will have accumulated and the slower the resulting erosion rate at a basin scale. In contrast, more rapid rates in the turnover of bedrock to sediment and transport to and through the fluvial system, the less accumulated ^{10}Be and the higher the resulting erosion rate. This difference in the residence time in the near surface is likely encoded in the changes in OSL sensitivity between the modern and Late Pleistocene sediments of High Creek.

Sawakuchi et al. (2018) proposed that slower exhumation leads to longer duration of chemical weathering which may be related to the sensitization of quartz. The CW-OSL sensitivity in High Creek scales with magnetic susceptibility and chemical weathering intensity (Fig. 5B–D), although previous work has shown that exposure to chemical weathering alone does not cause quartz sensitization (Cao et al., 2022). The accumulation of magnetic material and leaching of mobile elements increases with the time that sediments spend within the weathering zone (An et al., 1991; Dinis et al., 2020; Li and Zhou, 2021). Therefore, in addition to ^{10}Be accumulation, magnetic susceptibility and chemical weathering indices are used as proxies for sediment residence time within the shallow critical zone. Taken in sum, all three metrics indicate that the modern sediment had a greater residence time in the critical zone compared to Late Pleistocene sediment and fresh bedrock samples. We refer to residence time as the sum duration in the weathering profile and during hillslope and fluvial storage and transport.

Our results indicate that the strongest difference in OSL sensitivity is seen between alluvium produced in end-member climate states in the catchment (Holocene versus Pleistocene). The climate change between the Late Pleistocene and Holocene in the High Creek catchment would have led to changes in the dominant type and rate of bedrock and sediment weathering and transport on hillslopes. During the Late Pleistocene, the cooler and effectively wetter conditions are expected to have caused greater physical weathering by periglacial processes, producing coarse-grained colluvium and more efficient hillslope transport (e.g., Anderson et al., 2013; West et al., 2013; Marshall et al., 2017,

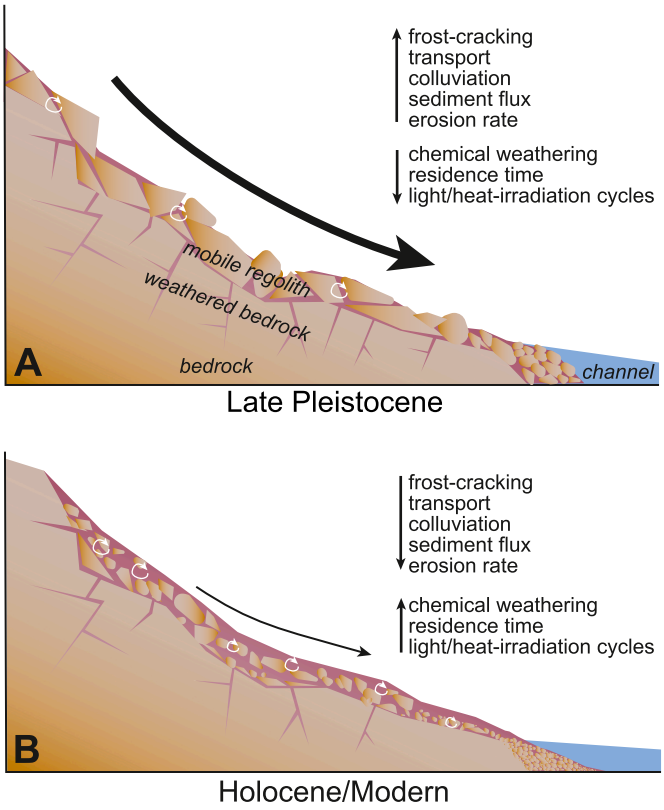

Fig. 6. Schematic diagram of a hillslope cross-section with hypothesized critical-zone processes between glacial Late Pleistocene (A) and the Holocene (B). In the Late Pleistocene, the cooler and effectively wetter conditions would cause greater physical weathering and increased erosion rates, which would produce coarse-grained colluvium and more efficient hillslope transport. During the Holocene, the warmer and more arid conditions would lead to less physical weathering and sediment production, lower erosion rates, and greater chemical weathering and quartz residence time in the critical zone. The arrows depict either increasing (up) or decreasing (down) rates of processes. White circular arrows depict soil mixing cycles within a shallow depth.

Fig. 6A). Pleistocene hillslopes were likely more weathering-limited, with less regolith storage. Higher erosion rates would result in rapid delivery of colluvium to the fluvial system in the Late Pleistocene and are expected to result in short residence times for sediment in the critical zone.

The transition to warmer conditions in the Holocene is projected to be accompanied by enhanced chemical weathering due to the rate dependence on temperature (e.g., White and Blum, 1995; Oliva et al., 2003; West et al., 2005; Ivory et al., 2014). Catchment-averaged erosion rates, chemical weathering indices, and magnetic susceptibility are consistent with this suggestion, as the modern alluvial sediments show slower erosion rates and greater leaching of mobile elements, the result of longer residence time in the weathering zone. Moreover, decreased colluvial production in the Holocene may have also slowed the transport of grains from hillslopes to the fluvial system (e.g., Anderson et al., 2013), thus extending the residence time for quartz grains in shallow critical zone (Fig. 6B). Increased vegetation in the Holocene (e.g., Louderback and Rhode, 2009; Thompson et al., 2016) would further enhance trapping of colluvium along hillslopes. In fact, surface residence time has been shown to be coupled to Pleistocene climate cycles (Dosseto and Schaller, 2016) and this proposed conceptual model of changing ^{10}Be-derived erosion rates and hillslope process can explain the patterns in chemical weathering indices and magnetic susceptibility between the Late Pleistocene and the Holocene. We conclude that retention of modern sediments in the shallow critical zone causes the observed enhanced OSL sensitivity.

6.3. Processes responsible for enhanced luminescence in the critical zone

Our results from the High Creek catchment in northern Utah demonstrate that weakly luminescent grains derived from bedrock are sensitized by accumulated exposure to critical-zone processes during the Holocene but not during the Late Pleistocene. From a mechanistic point of view, this enhanced luminescence could be due to several factors, such as an increase in crystalline defects, a greater number of luminescence centers, a decrease in non-radiative recombination centers (Bailey, 2001), and/or opening of deep traps for electron capture. However, it is unlikely that additional defects were generated within the crystalline structure during the short time captured by this study (<20 kyr). Instead, the sensitization is likely due to the accumulated number and duration of surface-exposure cycles experienced by the grains. The exposure of quartz grains to optical and thermal energy at the Earth's surface can lead to the clearing of deep traps and opening of recombination centers, both of which enhance OSL sensitivity (e.g., Moska and Murray, 2006; Pietsch et al., 2008; Mineli et al., 2021).

Important critical-zone processes that modulate the movement and mixing of hillslope materials include soil-creep, bioturbation, and tree-throw. These processes will lead to the repeated exposure of grains at the land surface as they slowly move downslope by diffusive processes (e.g., Heimsath et al., 2002; Wilkinson et al., 2009; Brown, 2020; Gray et al., 2020). Moreover, the chance of grain exposure at the surface is increased in thin soils, characteristic of modern hillslope conditions because mixing efficiency is depth dependent (Gray et al., 2020). In addition, longer residence time in the active weathering zone would cause more exposure to ionizing radiation which may promote physical damage within the quartz (e.g., Sawakuchi et al., 2018).

Exposure to the heat from wildfire is another important critical-zone process that can enhance quartz OSL sensitivity (e.g., Phinney, 2022; Zhang et al., 2023b). Records from the region suggest an increase in fire activity during the Holocene (e.g., Minckley et al., 2007; Brugger and Rhode, 2020). If fire activity increased in the High Creek catchment during the Holocene, then the greater residence time in the critical zone would expose grains residing at and near the surface to a greater cumulative number of fires, which may further enhance the OSL sensitivity.

A notable finding of this study is that OSL sensitivity within sediment may be encoded within a timeframe of 17 kyr (age of the delta) or less, whereas the catchment-averaged erosion signal derived from ^{10}Be requires a longer duration to be reflected in the sediment's^{10}Be inventory. This discrepancy in integration time is particularly evident in the sample collected from the upper South Fork, where quartz OSL sensitivity has been enhanced, yet the ^{10}Be inventory continues to indicate higher erosion rates (low ^{10}Be accumulation), likely attributable to Pleistocene glaciation. This underscores the potential of quartz OSL sensitivity as a tool for monitoring hillslope and critical zone processes.

7. Conclusions

Our results indicate that the Late Pleistocene alluvium has low OSL sensitivity that is similar to the bedrock source, but that the modern alluvium has enhanced luminescence properties with no clear relationship to bedrock source. We suggest that the observed differences in OSL sensitivity are due to changes in the rates and types of critical-zone processes in response to different mean climate states between the Late Pleistocene and Holocene. The similarity in OSL sensitivity between the Late Pleistocene alluvium and the bedrock quartzites implies that surface processes during the last glacial period did not lead to enhanced OSL sensitivity. In contrast, Holocene sediments show lower catchment-averaged erosion rates, increased intensity in chemical weathering, and greater magnetic susceptibility compared to the Pleistocene alluvium, suggesting that modern sediment supplied to the stream has maintained longer residence time on hillslopes. We conclude that the enhancement of the OSL sensitivity in the modern samples is due to the climate-

mediated increase in sediment exposure to ionizing radiation, sunlight, fires, and other processes during residence in the shallow critical zone. As such, differences between mean climate states in chemical or physical weathering rates and the related sediment mixing by critical zone processes, appear to be reflected in the luminescence properties of quartz sand. Additionally, results of this study suggests that it requires less time to encode changes in OSL sensitivity compared to ^{10}Be derived erosion rates. Findings within this study provide support for the use and further development of OSL sensitivity as a proxy for hillslope processes, weathering, erosion rates, and residence time in the critical zone.

CRediT authorship contribution statement

Natalie M. Tanski: Writing – original draft, Methodology, Investigation, Funding acquisition, Formal analysis, Data curation, Conceptualization. **Tammy M. Rittenour:** Writing – review & editing, Validation, Supervision, Funding acquisition, Conceptualization. **Francesco Pavano:** Writing – review & editing, Data curation. **Frank Pazzaglia:** Writing – review & editing, Funding acquisition, Data curation. **Jenna Mills:** Formal analysis, Data curation. **Lee B. Corbett:** Writing – review & editing, Data curation. **Paul Bierman:** Writing – review & editing, Data curation.

Declaration of competing interest

The authors declare that they have no known competing financial interests or personal relationships that could have appeared to influence the work reported in this paper.

Data availability

Data will be made available on request.

Acknowledgements

This work was supported by the Desert Research Institute Jonathan O. Davis Research Grant to Tanski and by NSF-EAR-1904278 to Rittenour and NSF-EAR-1904262 to Pazzaglia. Sample preparation, data analysis, and manuscript preparation in part supported by NSF-EAR-1735676 and NSF-EAR- 2300560 to Bierman. Laurent Roberge, Nicole Gasparini, and Leia Barnes are thanked for their assistance in sample collection and processing. We would like to thank two anonymous reviewers for their constructive comments which have significantly improved this study.

Appendix A. Supplementary data

Supplementary data to this article can be found online at https://doi.org/10.1016/j.quageo.2024.101613.

References

Aitken, M., 1998. Introduction to optical dating: the dating of Quaternary sediments by the use of photon-stimulated luminescence.

Alexanderson, H., 2022. Luminescence characteristics of Scandinavian quartz, their connection to bedrock provenance and influence on dating results. Quat. Geochronol. 69, 101272. https://doi.org/10.1016/J.QUAGEO.2022.101272.

An, Z., Kukla, G.J., Porter, S.C., Xiao, J., 1991. Magnetic susceptibility evidence of monsoon variation on the Loess Plateau of central China during the last 130,000 years. Quat. Res. 36, 29–36. https://doi.org/10.1016/0033-5894(91)90015-W.

Anderson, R.S., Anderson, S.P., Tucker, G.E., 2013. Rock damage and regolith transport by frost: an example of climate modulation of the geomorphology of the critical zone. Earth Surf. Process. Landforms 38, 299–316. https://doi.org/10.1002/esp.3330.

Bailey, R.M., 2001. Towards a general kinetic model for optically and thermally stimulated luminescence of quartz. Radiat. Meas. 33, 17–45. https://doi.org/10.1016/S1350-4487(00)00100-1.

Balco, G., Stone, J.O., Lifton, N.A., Dunai, T.J., 2008. A complete and easily accessible means of calculating surface exposure ages or erosion rates from 10Be and 26Al measurements. Quat. Geochronol. 3, 174–195. https://doi.org/10.1016/j.quageo.2007.12.001.

Belanger, B.K., Amidon, W.H., Laabs, B.J.C., Munroe, J.S., Quirk, B.J., 2022. Modelling climate constraints on the formation of pluvial Lake Bonneville in the great basin, United States. J. Quat. Sci. 37, 478–488. https://doi.org/10.1002/JQS.3394.

Benson, L.V., Thompson, R.S., 1987. Lake-level variation in the lahontan basin for the past 50,000 years. Quat. Res. 28, 69–85. https://www.researchgate.net/publication/240323138.

Bierman, P., Steig, E.J., 1996. Estimating rates of denudation using cosmogenic isotope abundances in sediment. Earth Surf. Process. Landforms 21, 125–139. https://doi.org/10.1002/(sici)1096-9837(199602)21:2<125::aid-esp511>3.0.co;2-8.

von Blanckenburg, F., 2005. The control mechanisms of erosion and weathering at basin scale from cosmogenic nuclides in river sediment. Earth Planet Sci. Lett. 237, 462–479. https://doi.org/10.1016/j.epsl.2005.06.030.

Bøtter-Jensen, L., Agersnap Larsen, N., Mejdahl, V., Poolton, N.R.J., Morris, M.F., McKeever, S.W.S., 1995. Luminescence sensitivity changes in quartz as a result of annealing. Radiat. Meas. 24, 535–541. https://doi.org/10.1016/1350-4487(95)00006-Z.

Bøtter-Jensen, L., Andersen, C.E., Duller, G.A.T., Murray, A.S., 2003. Developments in radiation, stimulation and observation facilities in luminescence measurements. In: Radiation Measurements, vol. 37. Elsevier Ltd, pp. 535–541. https://doi.org/10.1016/S1350-4487(03)00020-9.

Brown, N.D., 2020. Which geomorphic processes can be informed by luminescence measurements? Geomorphology 367, 107296. https://doi.org/10.1016/j.geomorph.2020.107296.

Brown, E., Stallard, R.F., Larsen, M.C., Raisbeck, G.M., Yiou, F., 1995. EPSL Denudation rates determined from the accumulation of in situ-produced loBe in the Luquillo Experimental Forest, Puerto Rico. Earth Planet Sci. Lett. 129, 193–202.

Brugger, S.O., Rhode, D., 2020. Impact of Pleistocene–Holocene climate shifts on vegetation and fire dynamics and its implications for Prearchaic humans in the central Great Basin, USA. J. Quat. Sci. 35, 987–993. https://doi.org/10.1002/jqs.3248.

Buggle, B., Glaser, B., Hambach, U., Gerasimenko, N., Marković, S., 2011. An evaluation of geochemical weathering indices in loess–paleosol studies. Quat. Int. 240, 12–21. https://doi.org/10.1016/J.QUAINT.2010.07.019.

Bull, W., 1991. Geomorphic responses to climatic change. https://www.osti.gov/biblio/5603696 (accessed January 2022).

Bulur, E., Bùtter-Jensen, L., Murray, A.S., 2000. Optically Stimulated Luminescence from Quartz Measured Using the Linear Modulation Technique. www.elsevier.com/locate/radmeas.

Cao, Z., Jiang, Y., Xu, J., Zhao, J., Zhao, C., 2022. Luminescence sensitivity of quartz from rocks under in situ chemical weathering conditions. Front. Earth Sci. 10, 1–14. https://doi.org/10.3389/feart.2022.940212.

Capaldi, T.N., Rittenour, T.M., Nelson, M.S., 2022. Downstream changes in quartz OSL sensitivity in modern river sand reflects sediment source variability: case studies from Rocky Mountain and Andean rivers. Quat. Geochronol. 71 https://doi.org/10.1016/j.quageo.2022.101317.

Chithambo, M.L., Preusser, F., Ramseyer, K., Ogundare, F.O., 2007. Time-resolved luminescence of low sensitivity quartz from crystalline rocks. Radiat. Meas. 42, 205–212. https://doi.org/10.1016/j.radmeas.2006.07.005.

Clift, P.D., 2006. Controls on the erosion of Cenozoic Asia and the flux of clastic sediment to the ocean. Earth Planet Sci. Lett. 241, 571–580. https://doi.org/10.1016/j.epsl.2005.11.028.

Corbett, L.B., Bierman, P.R., Rood, D.H., 2016. An approach for optimizing in situ cosmogenic 10Be sample preparation. Quat. Geochronol. 33, 24–34. https://doi.org/10.1016/j.quageo.2016.02.001.

Dave, A.K., Timar-Gabor, A., Scardia, G., Safaraliev, N., Fitzsimmons, K.E., 2022. Variation in luminescence characteristics and paramagnetic defect centres in fine-grained quartz from a loess-palaeosol sequence in Tajikistan: implications for provenance studies in aeolian environments. Front. Earth Sci. 10 https://doi.org/10.3389/feart.2022.835281.

DeGraff, J., 1976. Quaternary geomorphic features of the Bear River range, north-central Utah. https://digitalcommons.usu.edu/etd/6658/ (accessed November 2022).

Dinis, P.A., Garzanti, E., Hahn, A., Vermeesch, P., Cabral-Pinto, M., 2020. Weathering indices as climate proxies. A step forward based on Congo and SW African river muds. Earth Sci. Rev. 201, 103039 https://doi.org/10.1016/j.earscirev.2019.103039.

Dinis, P., Garzanti, E., Vermeesch, P., Huvi, J., 2017. Climatic zonation and weathering control on sediment composition (Angola). Chem. Geol. 467, 110–121. https://doi.org/10.1016/J.CHEMGEO.2017.07.030.

Dosseto, A., Schaller, M., 2016. The erosion response to Quaternary climate change quantified using uranium isotopes and in situ-produced cosmogenic nuclides. Earth Sci. Rev. 155, 60–81. https://doi.org/10.1016/j.earscirev.2016.01.015.

Dover, James H., 2007. Geologic Map of the Logan 30' X 60' Quadrangle, Cache and Rich Counties, Utah, and Lincoln and Uinta Counties. Wyoming. MP-06-8dm. UGS. 1:100,000 scale.

Durcan, J.A., Duller, G.A.T., 2011. The fast ratio: a rapid measure for testing the dominance of the fast component in the initial OSL signal from quartz. Radiat. Meas. 46, 1065–1072. https://doi.org/10.1016/j.radmeas.2011.07.016.

Durcan, J.A., King, G.E., Duller, G.A.T., 2015. DRAC: dose rate and age calculator for trapped charge dating. Quat. Geochronol. 28, 54–61. https://doi.org/10.1016/j.quageo.2015.03.012.

Evans, J.P., 1991. Structural Setting of Seismicity in Northern Utah: Utah Geological Survey Contract Report, vol. 91. Utah Geological Survey.

Fitzsimmons, K.E., 2011. An assessment of the luminescence sensitivity of australian quartz with respect to sediment history. Geochronometria 38, 199–208. https://doi.org/10.2478/s13386-011-0030-9.
Fitzsimmons, K.E., Rhodes, E.J., Barrows, T.T., 2010. OSL dating of southeast Australian quartz: a preliminary assessment of luminescence characteristics and behaviour. Quat. Geochronol. 5, 91–95. https://doi.org/10.1016/j.quageo.2009.02.009.
Forte, A.M., Whipple, K.X., 2019. Short communication: the topographic analysis kit (TAK) for TopoToolbox. Earth Surf. Dyn. 7, 87–95. https://doi.org/10.5194/esurf-7-87-2019.
Fuchs, M., Owen, L.A., 2008. Luminescence dating of glacial and associated sediments: review, recommendations and future directions. Boreas 37, 636–659. https://doi.org/10.1111/J.1502-3885.2008.00052.X.
Galbraith, R.F., Roberts, R.G., 2012. Statistical aspects of equivalent dose and error calculation and display in OSL dating: an overview and some recommendations. Quat. Geochronol. 11, 1–27. https://doi.org/10.1016/J.QUAGEO.2012.04.020.
Galbraith, R.F., Roberts, R.G., Laslett, G.M., Yoshida, H., Olley, J.M., 1999. Optical dating of single and multiple grains of quartz from Jinmium rock shelter, northern Australia: Part I, experimental design and statistical models. Archaeometry 41, 339–364. https://doi.org/10.1111/J.1475-4754.1999.TB00987.X.
Galloway, R.B., 2002. Luminescence lifetimes in quartz: dependence on annealing temperature prior to beta irradiation. Radiat. Meas. 35, 67–77. https://doi.org/10.1016/S1350-4487(01)00258-X.
García, A.F., Stokes, M., 2006. Late Pleistocene highstand and recession of a small, high-altitude pluvial lake, Jakes Valley, central Great Basin, USA. Quat. Res. 65, 179–186. https://doi.org/10.1016/j.yqres.2005.08.025.
Garzanti, E., Padoan, M., Setti, M., López-Galindo, A., Villa, I.M., 2014. Provenance versus weathering control on the composition of tropical river mud (southern Africa). Chem. Geol. 366, 61–74. https://doi.org/10.1016/J.CHEMGEO.2013.12.016.
Gilbert, G.K., 1890. Lake Bonneville. US Geological Survey Monograph 1, Vol. 1.
Gilbert, G.K., 1877. Report on the Geology of the Henry Mountains. https://doi.org/10.5962/bhl.title.51652.
Gliganic, L.A., Cohen, T.J., Meyer, M., Molenaar, A., 2017. Variations in luminescence properties of quartz and feldspar from modern fluvial sediments in three rivers. Quat. Geochronol. 41, 70–82. https://doi.org/10.1016/J.QUAGEO.2017.06.005.
Godsey, H.S., Currey, D.R., Chan, M.A., 2005. New evidence for an extended occupation of the Provo shoreline and implications for regional climate change, Pleistocene Lake Bonneville, Utah, USA. Quat. Res. 63, 212–223. https://doi.org/10.1016/J.YQRES.2005.01.002.
Godsey, H.S., Oviatt, C.G., Miller, D.M., Chan, M.A., 2011. Stratigraphy and chronology of offshore to nearshore deposits associated with the Provo shoreline, Pleistocene Lake Bonneville, Utah. Palaeogeogr. Palaeoclimatol. Palaeoecol. 310, 442–450. https://doi.org/10.1016/j.palaeo.2011.08.005.
Goswami, K., Panda, S.K., Alappat, L., Chauhan, N., 2023. Luminescence for sedimentary provenance quantification in river basins: a methodological advancement. Quat. Geochronol., 101488 https://doi.org/10.1016/j.quageo.2023.101488.
Granger, D.E., Kirchner, J.W., Finkel, R., 1996. Spatially averaged long-term erosion rates measured from in situ-produced cosmogenic nuclides in alluvial sediment. Geology 104, 249–257.
Gray, H.J., Jain, M., Sawakuchi, A.O., Mahan, S.A., Tucker, G.E., 2019. Luminescence as a sediment tracer and provenance tool. Rev. Geophys. 57, 987–1017. https://doi.org/10.1029/2019RG000646.
Gray, H.J., Keen-Zebert, A., Furbish, D.J., Tucker, G.E., Mahan, S.A., 2020. Depth-dependent soil mixing persists across climate zones. Proc. Natl. Acad. Sci. USA 117, 8750–8756. https://doi.org/10.1073/pnas.1914140117/-/DCSupplemental.
Gunderson, K.L., Kodama, K.P., Anastasio, D.J., Pazzaglia, F.J., 2012. Rock-magnetic Cyclostratigraphy for the Late Pliocene-Early Pleistocene Stirone Section, Northern Apennine Mountain Front, Italy, vol. 373. Geological Society Special Publication, pp. 309–323. https://doi.org/10.1144/SP373.8.
Guralnik, B., et al., 2015. OSL-thermochronometry using bedrock quartz: a note of caution. Quat. Geochronol. 25, 37–48. https://doi.org/10.1016/j.quageo.2014.09.001.
Hashimoto, T., Yamaguchi, T., Fujita, H., Yanagawa, Y., 2003. Comparison of infrared spectrometric characteristics of Al-OH impurities and thermoluminescence patterns in natural quartz slices at temperatures below 0 °C. Radiat. Meas. 37, 479–485. https://doi.org/10.1016/S1350-4487(03)00061-1.
Heimsath, A.M., Burke, B.C., 2013. The impact of local geochemical variability on quantifying hillslope soil production and chemical weathering. Geomorphology 200, 75–88. https://doi.org/10.1016/j.geomorph.2013.03.007.
Heimsath, A.M., Chappell, J., Danièe, N.A.S., Questiaux, G., 2002. Creeping soil: geology, 111. http://pubs.geoscienceworld.org/gsa/geology/article-pdf/30/2/111/3522811/i0091-7613-30-2-111.pdf.
Heinrich, H., 1988. Origin and consequences of cyclic ice rafting in the Northeast Atlantic Ocean during the past 130,000 years. Quat. Res. 29, 142–152. https://doi.org/10.1016/0033-5894(88)90057-9.
Hu, D., Clift, P.D., Böning, P., Hannigan, R., Hillier, S., Blusztajn, J., Wan, S., Fuller, D.Q., 2013. Holocene evolution in weathering and erosion patterns in the Pearl River delta. G-cubed 14, 2349–2368. https://doi.org/10.1002/ggge.20166.
Huntley, D., Godfrey-Smith, D., Nature, M.T.-, 1985. Optical Dating of Sediments. Springer. https://link.springer.com/content/pdf/10.1038/313105a0.pdf. ed April 2020).
Ivory, S.J., McGlue, M.M., Ellis, G.S., Lézine, A.M., Cohen, A.S., Vincens, A., 2014. Vegetation controls on weathering intensity during the last deglacial transition in southeast Africa. PLoS One 9. https://doi.org/10.1371/journal.pone.0112855.
Jeong, G.Y., Choi, J.H., 2012. Variations in quartz OSL components with lithology, weathering and transportation. Quat. Geochronol. 10, 320–326. https://doi.org/10.1016/j.quageo.2012.02.023.
Kitis, G., Pagonis, V., 2008. Computerized curve deconvolution analysis for LM-OSL. Radiat. Meas. 43, 737–741. https://doi.org/10.1016/j.radmeas.2007.12.055.
Klasen, N., Fiebig, M., Preusser, F., Reitner, J.M., Radtke, U., 2007. Luminescence dating of proglacial sediments from the Eastern Alps. Quat. Int. 164–165, 21–32. https://doi.org/10.1016/j.quaint.2006.12.003.
Kreutzer, S., et al., 2023. Package "Luminescence. https://orcid.org/0000-0002-6375-9108.
Larsen, R.B., Henderson, I., Ihlen, P.M., Jacamon, F., 2004. Distribution and petrogenetic behaviour of trace elements in granitic pegmatite quartz form South Norway. Contrib. Mineral. Petrol. 147, 615–628. https://doi.org/10.1007/s00410-004-0580-4.
Li, S.H., Wintle, A.G., 1992. Luminescence sensitivity change due to bleaching of sediments: international journal of radiation applications and instrumentation. Part D. Nucl. Tracks Radiat. Meas. 20, 567–573. https://doi.org/10.1016/1359-0189(92)90006-H.
Li, Y., Zhou, L., 2021. Variations of thermally and optically stimulated luminescence sensitivity of loess and pedocomplex samples from southern Tajikistan. Central Asia: Geochronometria 48, 242–252. https://doi.org/10.1515/geochr-2015-0118.
Louderback, L.A., Rhode, D.E., 2009. 15,000 Years of vegetation change in the Bonneville basin: the Blue Lake pollen record. Quat. Sci. Rev. 28, 308–326. https://doi.org/10.1016/j.quascirev.2008.09.027.
Louderback, L.A., Rhode, D., Madsen, D.B., Metcalf, M., 2015. Rapid vegetation shifts in the uinta mountains (Utah and Wyoming, USA) during the late pleistocene and Holocene. Palaeogeogr. Palaeoclimatol. Palaeoecol. 438, 327–343. https://doi.org/10.1016/j.palaeo.2015.08.026.
Lu, T., Sun, J., Feathers, J.K., Sun, D., 2021. Spatiotemporal variations and implications of luminescence sensitivity of quartz grains on the Chinese Loess Plateau since the last interglaciation. Quaternary Research (United States) 99, 190–203. https://doi.org/10.1017/qua.2020.53.
Lü, T., Sun, J., Li, S.H., Gong, Z., Xue, L., 2014. Vertical variations of luminescence sensitivity of quartz grains from loess/paleosol of Luochuan section in the central Chinese Loess Plateau since the last interglacial. Quat. Geochronol. 22, 107–115. https://doi.org/10.1016/J.QUAGEO.2014.04.004.
Lyle, M., Heusser, L., Ravelo, C., Yamamoto, M., Barron, J., Diffenbaugh, N.S., Herbert, T., Andreasen, D., 2012. Out of the tropics: the pacific, great basin lakes, and late pleistocene water cycle in the western United States. Science 337, 1629–1633. https://doi.org/10.1126/science.1218390.
Marshall, J.A., Roering, J.J., Bartlein, P.J., Gavin, D.G., Granger, D.E., Rempel, A.W., Praskievicz, S.J., Hales, T.C., 2015. Frost for the trees: did climate increase erosion in unglaciated landscapes during the late Pleistocene? Sci. Adv. 1 https://doi.org/10.1126/sciadv.1500715.
Marshall, J.A., Roering, J.J., Gavin, D.G., Granger, D.E., 2017. Late quaternary climatic controls on erosion rates and geomorphic processes in western Oregon. USA: Bull. Geol. Soc. Am. 129, 715–731. https://doi.org/10.1130/B31509.1.
Marshall, J.A., Roering, J.J., Rempel, A.W., Shafer, S.L., Bartlein, P.J., 2021. Extensive frost weathering across unglaciated north America during the last glacial maximum. Geophys. Res. Lett. 48 https://doi.org/10.1029/2020GL090305.
Matsubara, Y., Howard, A.D., 2009. A spatially explicit model of runoff, evaporation, and lake extent: application to modern and late Pleistocene lakes in the Great Basin region, western United States. Water Resour. Res. 45, 1–18. https://doi.org/10.1029/2007WR005953.
McCalpin, J.P., 1994. NEOTECTONIC DEFORMATION along the EAST CACHE FAULT ZONE, CACHE COUNTY, UTAH Special Study 83 UTAH GEOLOGICAL SURVEY UTAH DEPARTMENT of NATURAL RESOURCES.
Miller, D.M., Wahl, D.B., McGeehin, J.P., Rosario, J., Oviatt, C.G., Anderson, L., Presnetsova, L., 2015. Limiting age for the Provo shoreline of Lake Bonneville. Quat. Int. 387, 99–105. https://doi.org/10.1016/j.quaint.2015.01.001.
Minckley, T.A., Whitlock, C., Bartlein, P.J., 2007. Vegetation, fire, and climate history of the northwestern Great Basin during the last 14,000 years. Quat. Sci. Rev. 26, 2167–2184. https://doi.org/10.1016/j.quascirev.2007.04.009.
Mineli, T.D., Sawakuchi, A.O., Guralnik, B., Lambert, R., Jain, M., Pupim, F.N., Rio, I. del, Guedes, C.C.F., Nogueira, L., 2021. Variation of luminescence sensitivity, characteristic dose and trap parameters of quartz from rocks and sediments. Radiat. Meas. 144 https://doi.org/10.1016/j.radmeas.2021.106583.
Moska, P., Murray, A.S., 2006. Stability of the quartz fast-component in insensitive samples. Radiat. Meas. 41, 878–885. https://doi.org/10.1016/j.radmeas.2006.06.005.
Munroe, J.S., Laabs, B.J.C., 2013. Temporal correspondence between pluvial lake highstands in the southwestern US and Heinrich Event 1. J. Quat. Sci. 28, 49–58. https://doi.org/10.1002/jqs.2586.
Murray, A., Arnold, L.J., Buylaert, J.-P., Guérin, G., Qin, J., Singhvi, A.K., Smedley, R., Thomsen, K.J., 2021. Optically stimulated luminescence dating using quartz. Nature Reviews Methods Primers 1. https://doi.org/10.1038/s43586-021-00068-5.
Murray, A.S., Wintle, A.G., 2000. Luminescence dating of quartz using an improved single-aliquot regenerative-dose protocol. Radiat. Meas. 32, 57–73. https://doi.org/10.1016/S1350-4487(99)00253-X.
National Research Council (NRC), 2001. Basic Research Opportunities in Earth Science. Washington D C: National Academy Press.
Nelson, M.S., Eppes, M.C., Rittenour, T.M., 2022. Quartz luminescence sensitivity from sediment versus bedrock in highly weathered soils of the Piedmont of North Carolina, south-eastern USA. Quat. Geochronol. 72, 101343 https://doi.org/10.1016/J.QUAGEO.2022.101343.

Nesbitt, H.W., Markovics, G., Price, R.C., 1980. Chemical processes affecting alkalis and alkaline earths during continental weathering. Geochem. Cosmochim. Acta 44, 1659–1666.
Nesbitt, H., Young, G., 1982. Early Proterozoic climates and plate motions inferred from major element chemistry of lutites. Nature 299, 715–717. https://www.nature.com/articles/299715a0. November 2022.
Nian, X., Zhang, W., Qiu, F., Qin, J., Wang, Z., Sun, Q., Chen, J., Chen, Z., Liu, N., 2019. Luminescence characteristics of quartz from Holocene delta deposits of the Yangtze River and their provenance implications. Quat. Geochronol. 49, 131–137. https://doi.org/10.1016/j.quageo.2018.04.010.
Nishiizumi, K., Imamura, M., Caffee, M.W., Southon, J.R., Finkel, R.C., McAninch, J., 2007. Absolute calibration of 10Be AMS standards. Nucl. Instrum. Methods Phys. Res. Sect. B Beam Interact. Mater. Atoms 258, 403–413. https://doi.org/10.1016/j.nimb.2007.01.297.
Oliva, P., Viers, J., Dupré, B., 2003. Chemical weathering in granitic environments. Chem. Geol. 202, 225–256. https://doi.org/10.1016/j.chemgeo.2002.08.001.
Oviatt, C.G., 2015. Chronology of Lake Bonneville, 30,000 to 10,000 yr B.P. Quat. Sci. Rev. 110, 166–171. https://doi.org/10.1016/j.quascirev.2014.12.016.
Oviatt, C.G., Currey, D.R., Sack, D., 1992. Radiocarbon Chronology of Lake.
Palamakumbura, R.N., Robertson, A.H.F., Kinnaird, T.C., Van Calsteren, P., Kroon, D., Tait, J.A., 2016. Quantitative Dating of Pleistocene Deposits of the Kyrenia Range, Northern Cyprus: Implications for Timing, Rates of Uplift and Driving Mechanisms. https://doi.org/10.6084/m9.figshare.c.3260977.
Phinney, A.I., 2022. Investigating the Use of Quartz Luminescence and Rock-Color Alteration to Characterize Wildfire Exposure; Applied to the 2020 Mangum Fire, Kaibab Plateau, Arizona. Utah State University (Masters Thesis.
Pietsch, T.J., Olley, J.M., Nanson, G.C., 2008. Fluvial transport as a natural luminescence sensitiser of quartz. Quat. Geochronol. 3, 365–376. https://doi.org/10.1016/j.quageo.2007.12.005.
Preusser, F., Chithambo, M.L., Götte, T., Martini, M., Ramseyer, K., Sendezera, E.J., Susino, G.J., Wintle, A.G., 2009. Quartz as a natural luminescence dosimeter. Earth Sci. Rev. 97, 184–214. https://doi.org/10.1016/J.EARSCIREV.2009.09.006.
Rhodes, E.J., 2000. Observations of thermal transfer OSL signals in glacigenic quartz. Radiat. Meas. 32, 595–602. https://doi.org/10.1016/S1350-4487(00)00125-6.
Sawakuchi, A.O., et al., 2018. Luminescence of quartz and feldspar fingerprints provenance and correlates with the source area denudation in the Amazon River basin. Earth Planet Sci. Lett. 492, 152–162. https://doi.org/10.1016/J.EPSL.2018.04.006.
Sawakuchi, A.O., Blair, M.W., DeWitt, R., Faleiros, F.M., Hyppolito, T., Guedes, C.C.F., 2011. Thermal history versus sedimentary history: OSL sensitivity of quartz grains extracted from rocks and sediments. Quat. Geochronol. 6, 261–272. https://doi.org/10.1016/j.quageo.2010.11.002.
Schwanghart, W., Scherler, D., 2014. Short Communication: TopoToolbox 2 - MATLAB-based software for topographic analysis and modeling in Earth surface sciences. Earth Surf. Dyn. 2, 1–7. https://doi.org/10.5194/esurf-2-1-2014.
Souza, P.E., Pupim, F.N., Mazoca, C.E.M., Río, I. del, Mineli, T.D., Rodrigues, F.C.G., Porat, N., Hartmann, G.A., Sawakuchi, A.O., 2023. Quartz OSL sensitivity from dating data for provenance analysis of Pleistocene and Holocene fluvial sediments from lowland Amazonia. Quat. Geochronol. 74 https://doi.org/10.1016/j.quageo.2023.101422.
Stock, G.M., Frankel, K.L., Ehlers, T.A., Schaller, M., Briggs, S.M., Finkel, R.C., 2009. Spatial and temporal variations in denudation of the Wasatch Mountains, Utah, USA. Lithosphere 1, 34–40. https://doi.org/10.1130/L15.1.
Tajika, Y., Hashimoto, T., 2006. Correlation of blue-thermoluminescence (BTL) properties with some impurities in synthetic quartz. Radiat. Meas. 41, 809–812. https://doi.org/10.1016/j.radmeas.2006.05.014.
Thompson, R.S., Oviatt, C.G., Honke, J.S., McGeehin, J.P., 2016. Late quaternary changes in lakes, vegetation, and climate in the Bonneville basin reconstructed from sediment cores from great Salt Lake. In: Developments in Earth Surface Processes, vol. 20. Elsevier B.V., pp. 221–291. https://doi.org/10.1016/B978-0-444-63590-7.00011-1
Tsukamoto, S., Nagashima, K., Murray, A.S., Tada, R., 2011. Variations in OSL components from quartz from Japan sea sediments and the possibility of reconstructing provenance. Quat. Int. 234, 182–189. https://doi.org/10.1016/J.QUAINT.2010.09.003.
Wark, D.A., Watson, E.B., 2006. TitaniQ: a titanium-in-quartz geothermometer. Contrib. Mineral. Petrol. 152, 743–754. https://doi.org/10.1007/s00410-006-0132-1.
West, A.J., Galy, A., Bickle, M., 2005. Tectonic and climatic controls on silicate weathering. Earth Planet Sci. Lett. 235, 211–228. https://doi.org/10.1016/j.epsl.2005.03.020.
West, N., Kirby, E., Bierman, P., Slingerland, R., Ma, L., Rood, D., Brantley, S., 2013. Regolith production and transport at the susquehanna shale hills critical zone observatory, part 2: insights from meteoric10Be. J. Geophys. Res.: Earth Surf. 118, 1877–1896. https://doi.org/10.1002/jgrf.20121.
White, A.F., Blum, A.E., 1995. Effects of climate on chemical weathering in watersheds: water-rock interaction. Proc. symposium, Vladivostok 59, 57–60. https://doi.org/10.1201/9780203734049-13, 1995,.
Whitney, J.W., Harrington, C.D., 1993. Relict colluvial boulder deposits as paleoclimatic indicators in the Yucca Mountain region, southern Nevada. Geol. Soc. Am. Bull. 105, 1008–1018. http://pubs.geoscienceworld.org/gsa/gsabulletin/article-pdf/105/8/1008/3381707/i0016-7606-105-8-1008.pdf.
Wilkinson, M.T., Richards, P.J., Humphreys, G.S., 2009. Breaking ground: pedological, geological, and ecological implications of soil bioturbation. Earth Sci. Rev. 97, 257–272. https://doi.org/10.1016/j.earscirev.2009.09.005.
Wintle, A.G., Murray, A.S., 1999. Luminescence sensitivity changes in quartz. Radiat. Meas. 30, 107–118.
Zhang, A., et al., 2023a. Luminescence fingerprints fluvial sediment transport from the Tibetan Plateau to the Bangladesh Delta. Earth Planet Sci. Lett. 622 https://doi.org/10.1016/j.epsl.2023.118387.
Zhang, J., Li, S.H., Sun, J., Tongyan, L., Zhou, X., Hao, Q., 2023b. Quartz luminescence sensitivity variation in the Chinese loess deposits: the potential role of wildfires. J. Quat. Sci. 38, 49–60. https://doi.org/10.1002/jqs.3462.